Macromolecules

Article

pubs.acs.org/Macromolecules

Shapeshifting: Reversible Shape Memory in Semicrystalline Elastomers[⊥]

Jing Zhou,[†] Sara A. Turner,[†] Sarah M. Brosnan,[†] Qiaoxi Li,[†] Jan-Michael Y. Carrillo,[‡] Dmytro Nykypanchuk,[§] Oleg Gang,[§] Valerie S. Ashby,[†] Andrey V. Dobrynin,[‡] and Sergei S. Sheiko[†,*]

[†]Department of Chemistry, University of North Carolina at Chapel Hill, North Carolina 27599-3290, United States

[‡]Institute of Materials Science and Department of Physics, University of Connecticut, Storrs, Connecticut 06268, United States

[§]Center for Functional Nanomaterials, Brookhaven National Laboratory, Upton New York 11973, United States

Supporting Information

ABSTRACT: We present a general strategy for enabling reversible shape transformation in semicrystalline shape memory (SM) materials, which integrates three different SM behaviors: conventional one-way SM, two-way reversible SM, and one-way reversible SM. While two-way reversible shape memory (RSM) is observed upon heating and cooling cycles, the one-way RSM occurs upon heating only. Shape reversibility is achieved through partial melting of a crystalline scaffold which secures memory of a temporary shape by leaving a latent template for recrystallization. This behavior is neither mechanically nor structurally constrained, thereby allowing for multiple switching between encoded shapes without applying any external force, which was demonstrated for different shapes including hairpin, coil, origami, and a robotic gripper. Fraction of reversible strain increases with cross-linking density, reaching a maximum of *ca.* 70%, and then decreases at higher cross-linking densities. This behavior has been shown to correlate with efficiency of securing the temporary shape.

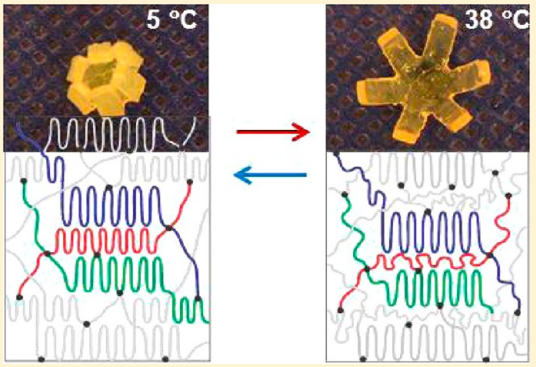

INTRODUCTION

Biological systems have the ability to program reversible shape changes in response to cues from their environment. While a variety of adaptive and stimuli-responsive materials like hydrogels,[1−6] liquid crystalline elastomers,[7−10] and shape memory materials,[11−21] have been developed, mimicking programmable behavior in a reversible way remains elusive. Shape memory polymers (SMPs) have two distinct advantages in this domain: First, SMPs can exhibit highly complex shape transformations (coils, knots, and origami) in response to a vast array of external stimuli.[13,14,22−25] Second, both initial and final shapes can be programmed and reprogrammed multiple times. However, these advantages are offset by the intrinsic irreversibility of shape memory transformations. In recent years, several groups have pioneered experimental studies enabling reversible shape memory.[10,26−28] Several strategies have been developed taking advantage of persistent external mechanical forces,[26,27,29,30] chemically heterogeneous structures,[28,31] and a broad meting transition.[32] Here we report a general approach for enabling reversible shifting between programmable shapes in semicrystalline elastomers with uniform chemical composition and without applying a persistent external force. This behavior stems from the correlated interplay between a crystalline scaffold and a network of chemical cross-links, each capable of encoding a distinct shape. Thermodynamically driven relaxation of extended polymer chains on heating is inverted by kinetically preferred pathways of polymer crystallization on cooling. The resulting reversible shape transformations are neither mechanically nor structurally constrained, thereby allowing for multiple switching between a multiplicity of encoded shapes without applying any external force. We conjecture that virtually all semicrystalline elastomers can be tailored to exploit this new mechanism of reversible shape memory transformation, considerably extending the range of practical applications, e.g., minimally invasive surgery[22,33] and hands-free packaging.[15,19]

Traditionally, polymer crystallites have been viewed as mechanical constructs embedded in amorphous networks that fasten a temporary shape. Those morphological constraints merely disappear on melting to recover the original shape. We have reconsidered this simple picture of semicrystalline elastomers and demonstrate that the network of crystallites plays an essential steering role in shape-memory behavior. In addition to counterbalancing the entropic elasticity of the amorphous network, crystallites encode an architectural scaffold within the semicrystalline polymer. Reversibility of shape transformations is achieved through partial melting of this

Received: November 8, 2013
Revised: February 12, 2014
Published: February 25, 2014

   dx.doi.org/10.1021/ma4023185 | *Macromolecules* 2014, 47, 1768−1776

Table 1. Composition and Physical Properties of Shape Memory Polymers

no.	polymer name	DP_n [b]	T_m (°C) [c]	ΔH_m (J/g) [c]	E (MPa) [d]	ν (mol/m^3) [d]	φ [e]
	Poly(octylene adipate) with Different Cross-Linking Densities						
1	POA[a]	6	23	21	7.9	900	0.99
2	POA	10	44	34	7.0	790	0.97
3	POA	11	47	44	5.4	610	0.97
4	POA	13	50	55	4.1	470	0.98
5	POA	20	59	70	1.5	170	0.93
	Polymers with Different Chemical Compositions						
6	POA copolymer	12	42	42	1.8	200	0.79
7	thio cross-linked POA copolymer	12	45	53	1.0	110	0.75
8	acrylate cross-linked POA copolymer	12	41	52	1.9	210	0.83
9	poly(octylene dodecanedioate)	6	55	52	3.7	420	0.98
10	POA (broad MW distribution)	10−15	41	41	5.5	620	0.98

[a]Poly(octylene adipate) in Figure S1a (Supporting Information). [b]Number-average degree of polymerization determined by proton NMR. [c]Temperature and enthalpy of melting measured by DSC, second heat at 5 °C/min. [d]Tensile storage modulus measured by DMA at T = 80 °C and f = 1 Hz. [d]Apparent cross-linking density calculated as ν=E/3RT. [e]Gel fraction is calculated as $\phi = m_d/m_0$, where m_0 is the initial mass and m_d is dry residue mass after Soxhlet extraction ($CHCl_3$ for 24 h) and drying in vacuum oven for 24 h.

scaffold, leaving a latent template behind, that in turn, inverts recovery of the original shape on cooling by steering crystallization along kinetically preferred pathways to replicate the scaffold. By controlling the melting and recrystallization processes, we can shift and expand the reversibility range without the need to change the elastomer's chemical structure. In sum, we have developed a general strategy for reversible shape memory (RSM) which can be applied to conventional semicrystalline elastomers. Our strategy integrates three different shape memory (SM) behaviors: conventional one-way SM, two-way RSM, and one-way RSM. We demonstrate that all of the aforementioned SM protocols can be realized in the same material and even in the same object. Furthermore, the relative contributions of the different strains (one-way SM, two-way RSM, and one-way RSM) to shape memory can be tuned by controlling the respective proportions of chemical cross-links and crystallites.

EXPERIMENTAL METHODS

Synthesis of Poly(octylene adipate). The procedure below describes the synthesis of polymer **2** (DP = 10, M_n = 2563 g/mol), while the other polymers from Table 1 have been synthesized in a similar way. A dry flask was charged with adipic acid (3.0 g, 20.53 mmol), 1,8-octanediol (3.242 g, 22.17 mmol), and scandium triflate catalyst (0.303 g, 0.62 mmol). The flask was nitrogen purged before heating the reaction to 80 °C. After 5 h, vacuum was lowered slowly to 40 Torr, and remained at that pressure for 24 h at which time it was pulled to 3 Torr for an additional 6 h. The polymerization was terminated by dissolving the polymer in $CHCl_3$, filtering, and precipitating in cold methanol (−78 °C). Final yield was 4.378 g of white solid. End group functionalization was performed according to procedures described elsewhere.[34]

Thermoset Elastomer Fabrication. End-capped POA (1.500 g, 0.55 mmol) was mixed with 1 mL chloroform in a dry vial, and then a drop (~0.2 μL) of 2,2-diethoxyacetophenone was added into the mixture. The vial was vortexed for 1 min then sonicated for 0.5 h. The mixture was poured into the mold and exposed to 365 nm light for 5 min. The thermoset elastomer was then removed from the mold and put under vacuum at a high temperature (70 °C, 20 Torr) overnight. The gel fraction was measured by a Soxhlet extractor using $CHCl_3$ as the extracting solution, extraction time 24h, and solvent evaporation occurred in the vacuum oven for 24 h. Apparent cross-linking density was calculated as =E/3RT, where E is the tensile storage modulus measured by DMA at strain ε = 0.1%, frequency f = 1 Hz, and temperature T = 80 °C. Table 1 summarizes chemical compositions and physical properties of the prepared elastomers.

Differential Scanning Calorimetry. DSC 220 from Seiko Instruments, Inc., was used, sample was measured at a heating and cooling rate of 5 K/min. The thermal data reported were obtained from the second heat. Enthalpy and crystal fraction were calculated through integration of area under the melting peak.

Dynamic Mechanical Analysis. RSA-G2 dynamic mechanical analyzer from TA Instruments was employed for both shape-programming and mechanical tests. A typical temperature ramp ranged from 0 to 80 °C at the same heating and cooling rates of 5 K/min. Given the kinetic nature of the crystallization process, we have maintained the same programming protocol for all samples to ensure that materials of the same composition have the same starting morphology. For shape programming, a dumbbell sample with an initial length of L_0 was heated to T = 70 °C (above melting transition) and was stretched to a strain around 20% (L_p) of the initial length. Then, the sample was quenched from 70 to 0 °C at a rate of 60 K/min and annealed at 0 °C for 5 min. Next, the sample was set to isoforce mode where the external force was set to be constantly at zero. To study two-way reversibility, the sample was heated to a preset partial melting temperature T_i at 5 K/min, 2 min was allowed to equilibrate at the intermediate sample length L_i. The sample was then cooled at a rate of 5 K/min back to 0 °C and the new length L_{2w} was measured. Total strain $\varepsilon_t = (L_p - L_0)/L_0$, two-way reversible strain $\varepsilon_{2w} = (L_{2w} - L_i)/L_0$, and fraction of reversible strain $\varepsilon_{2w}/\varepsilon_t$ were calculated from the sample dimensions measured experimentally. The sample dimensions were corrected for thermal expansion during the heating and cooling cycles, which was measured separately.

Atomic Force Microscopy. Topographic images of individual molecules were collected using a multimode Atomic Force Microscope with a NanoScope V controller in PeakForce QNM mode (Bruker). We used silicon cantilevers with a resonance frequency of 50−90 kHz and a spring constant of about 0.4 N/m.

Small Angle X-ray Scattering (SAXS). Measurements of SAXS spectra of shape memory elastomers were performed at the NSLS X9 beamline and on the CFN Bruker Nanostar SAXS instrument at Brookhaven National Laboratory using area detectors.

RESULTS AND DISCUSSION

To prove the concept and demonstrate its universality, a series of semicrystalline elastomers with systematically varied degree of cross-linking (ν) and melting temperature (T_m) have been synthesized and characterized (Table 1 and Supporting Information, Figure S1).[34] All polymers demonstrate conventional one-way irreversible SM observed upon complete melting. This behavior is relatively well understood[35,36] and not discussed in this paper dedicated solely to reversible shape memory (RSM). Figure 1 shows an experimental demon-

dx.doi.org/10.1021/ma4023185 | Macromolecules 2014, 47, 1768−1776

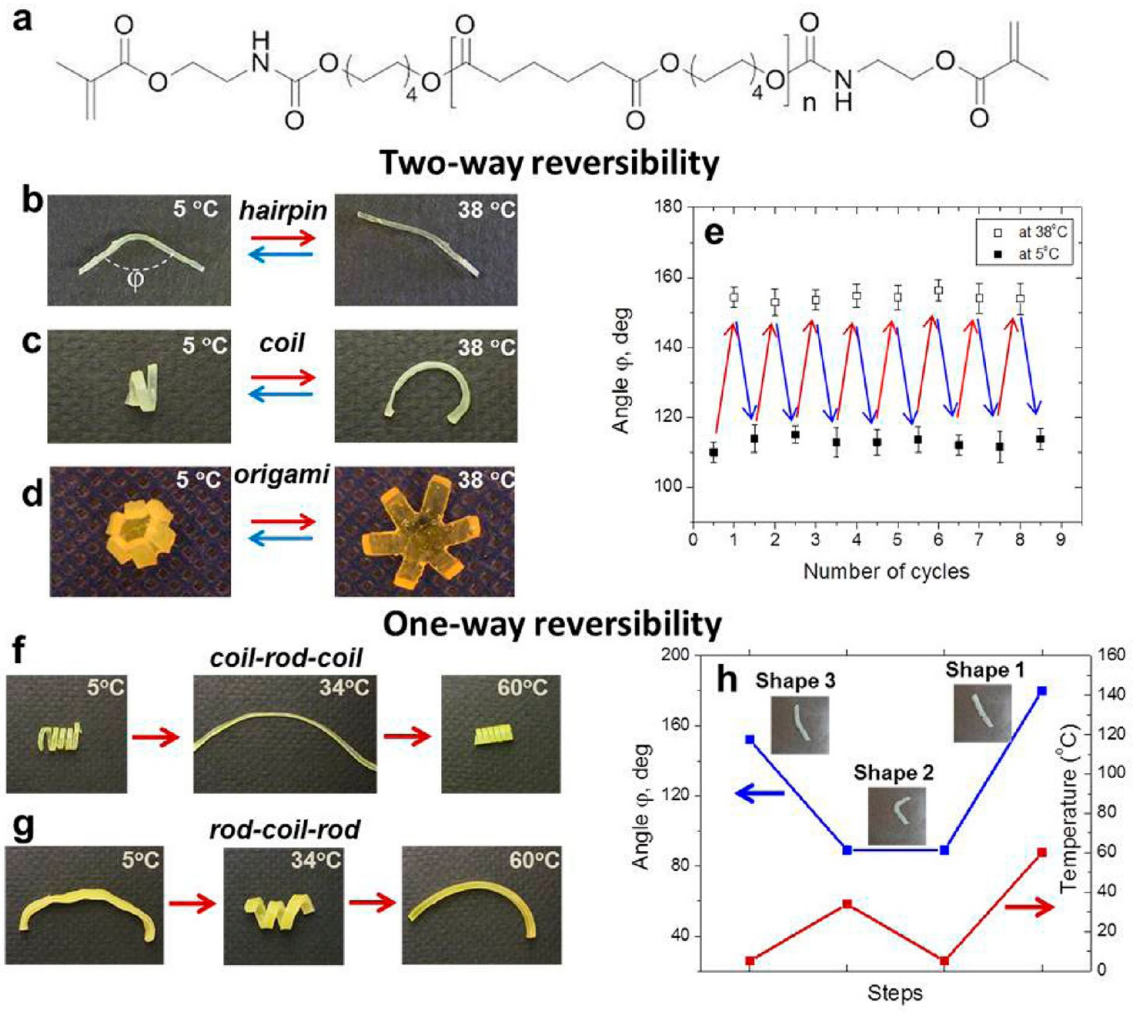

Figure 1. Two-way and one-way-reversible shape memory. (a) Chemical structure of poly(octylene adipate) (POA) oligomers used for the synthesis of shape-memory elastomers. Their cross-linking density and melting temperature were controlled by varying the degree of polymerization n of the oligomers and copolymerization (Table 1 and Supporting Information, Figure S1). (b–e) Examples of two-way reversible shape memory demonstrated by polymer 6 (ν = 200 mol/m^3, T_m = 42 °C), for three different shape transformations upon heating to 38 °C and subsequent cooling to 5 °C. (e) Reversible oscillations of the interior hairpin angle shown in panel b during eight consecutive heating–cooling cycles within the 5–38 °C temperature range. (f–h) One-way reversible shape transformations were observed during heating from 5 to 60 °C. While the two-way transformations may be repeated multiple times, the one-way reversibility occurs only once. (h) Temperature ramp and the corresponding variations of the interior angle of a hairpin sample which was programmed to perform one-way reversible bending.

stration of two different RSM concepts displayed by a poly(octylene adipate) (POA) elastomer (Figure 1a): (i) two-way reversible shape transformation upon heating–cooling cycles (Figure 1b–e) and (ii) one-way shape reversibility upon heating only (Figure 1f–h). In the first experiment (Figure 1b), a straight bar of the semicrystalline elastomer was programmed as a hairpin temporary shape by deforming the sample at a temperature of 60 °C and then quenching it to 5 °C. Subsequent heating to 38 °C and cooling to 5 °C resulted in reversible shape transformations of the hairpin between 115° and 155° angles, which occurred spontaneously without applying any external force. The angle oscillations were highly repeatable: upon consecutive heating and cooling cycles, the sample shape changed reversibly multiple times without losing memory of both angular shapes (Figure 1e). Similar reversible behavior was accomplished for a polymer coil (Figure 1c) and for the folding–unfolding of origami-like polymer sheets (Figure 1d; video in the Supporting Information). Note that the upper temperature, 38 °C, corresponds to partial melting of the crystalline phase (Table 1 and Supporting Information, Figure S2). As discussed below in more detail, partial melting allows for memory of the temporary shape to be preserved, so it may be restored upon subsequent cooling and recrystallization. Since degree of crystallinity depends on the cross-linking density and crystallization conditions, the temperature of partial melting T_i will be correlated with the corresponding volume fraction of the crystalline phase for each sample individually (Supporting Information, Figure S7).

In the second experiment (Figures 1f–h), a one-way reversible SM transformation was evoked in the same polymer (ν = 200 mol/m^3, T_m = 42 °C) by reprogramming the temporary shape at an elevated temperature corresponding to a partial molten state. As shown in Figure 1f, a sample having a temporary shape of a straight rod was heated to an intermediate temperature of T_i = 34 °C (substantially below T_m = 41 °C) and manually coiled into a new temporary shape. The new coil was then fixed by quenching to T_0 = 5 °C. Subsequent heating from T_0 = 5 °C to T_i = 34 °C and then to T = 60 °C, triggered

dx.doi.org/10.1021/ma4023185 | Macromolecules 2014, 47, 1768–1776

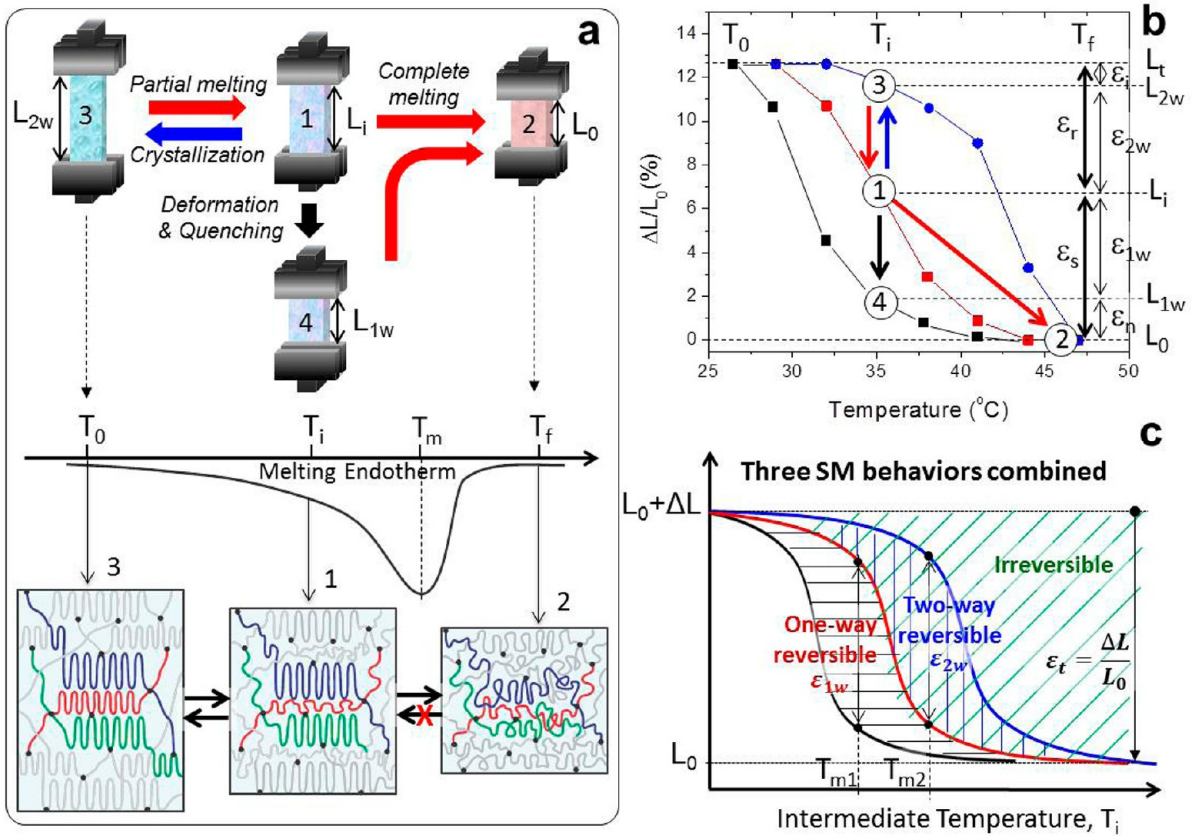

Figure 2. Interplay of reversible and irreversible shape-memory processes. A sample (thin film) of a POA elastomer (polymer **10** in Table 1, ν = 620 mol/m^3, T_m = 41 °C) was programmed by extension from the original length $L = L_0$ to a temporary length $L = L_t$ and quenching to a low temperature $T_0 \ll T_m$. (a) Partial melting of the extended sample at an intermediate temperature T_i causes partial contraction of the sample to an intermediate length $L = L_i$ (state 1), which is used as a starting state for three different shape-memory processes. (i) Subsequent heating to $T = T_f$ results in complete melting and irreversible recovery of the original length $L = L_0$ (state 2). (ii) Cooling and recrystallization causes reverse shape transformation (state 3), which can be repeated multiple times upon sequential cooling–heating cycles (two-way reversibility). (iii) From state 1, the sample can be reprogrammed by forced contraction and subsequent quenching at a low temperature (state 4). This process leads to one-way pseudoreversibility from state 4 to state 2 through the intermediate state 1. The cartoon underneath outlines a phenomenological mechanism of two-way reversible shape memory: In state 3, the extended shape is secured by a crystalline scaffold of oriented lamellae (Supporting Information, Figure S5c), which percolates through the entire sample and holds extended conformation of the polymer strands in the amorphous phase. Upon partial melting at $T = T_i$, the scaffold loses percolation triggering shape transformation (state 1). At state 1, the shape is controlled by clusters of remaining crystallites that may remain internally percolated (Supporting Information, Figure S10) and aligned. Upon cooling from state 1, the remaining crystallites serve as seeds and template for recrystallization of the previously molten crystallites at the original position, shape, and orientation. Replicating the original scaffold is the fastest pathway for recrystallization outlined by topological constraints imposed by chemical cross-links and crystallites. (2) Heating the sample significantly above the melting temperature T_m destroys the self-templating ability of the crystalline scaffold and makes shape recovery irreversible (state 2). (b) We have measured contraction of uniaxially stretched samples during heating and subtracted the length increase due to thermal expansion. Relative contributions of the SM processes depend on the temperature of partial melting T_i. With increasing T_i, the contribution of the one-way-RSM (ε_{1w}) decreases, while the contributions of the two-way RSM (ε_{2w}) and irreversible SM (ε_i) increases. When approaching the state of complete melting (state 2), shape recovery is largely irreversible and the total strain is dominated by ε_i. The other contributions into total strain $\varepsilon_t = \varepsilon_r + \varepsilon_s$ are explained in the main text. (c) Graphic representation of the relative contributions of the three different shape memory processes depending on the temperature of partial melting, i.e., intermediate temperature T_i. The maximum contributions of the one-way and two-way reversibilities are achieved at different temperatures $T_i = T_{m1}$ and $T_i = T_{m2}$, respectively. The SM transformation becomes irreversible upon complete melting at higher temperatures $T_i > T_f$.

a one-way transition from coil (second temporary shape) to rod (first temporary shape) and back to coil (permanent shape) (Figure 1f). In a similar way, we have demonstrated an opposite shape transformation, i.e. rod–coil–rod, using the same temperature ramp (Figure 1g). The reversible shape transformations in all these experiments were completely autonomous as they occurred without application of any external mechanical force. However, unlike the two-way RSM behavior, this one-way system required reprogramming of the temporary shape at an intermediate temperature T_i, which is analogous to the triple-shape memory protocol reported elsewhere.[16,37,38] In this pseudoreversible rod–coil–rod shape transformation, the permanent and second-temporary shapes are macroscopically identical; however, microscopic structures of these shapes are different.

Note that these three conceptually different SM processes were accomplished for the same material. However, their relative contributions into total sample deformation depend on temperature of partial melting (T_i) and cross-linking density of the chemical network (ν). Depending on the cross-linking density, samples attain different degree of crystallinity under the same crystallization conditions. Therefore, we shall first discuss

dx.doi.org/10.1021/ma4023185 | Macromolecules 2014, 47, 1768–1776

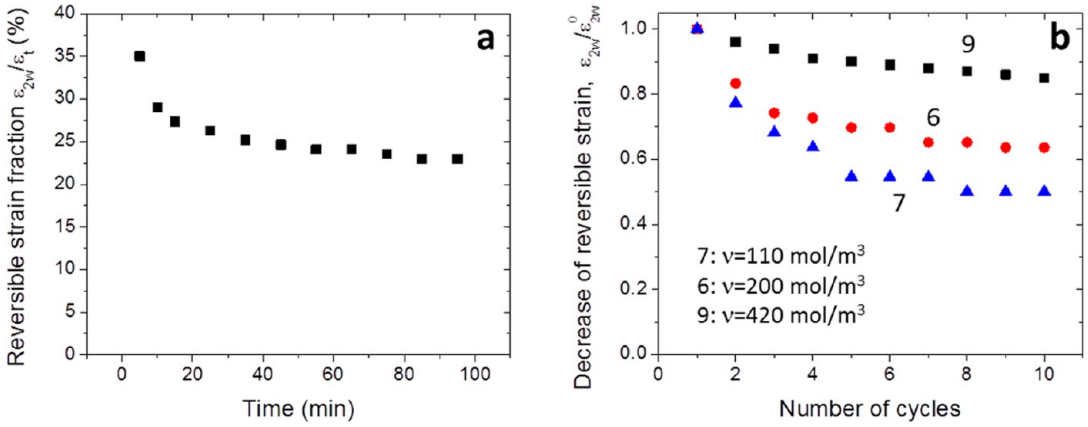

Figure 3. Effect of annealing and cross-linking density on two-way reversibility. (a) Initially, a dumbbell sample of polymer **6** (Table 1) was uniaxially stretched to ε_t = 20% strain at 80 °C and then quenched to 0 °C. The heating and cooling rates were 10 K/min. Subsequently, the sample were annealed T_i = 38 °C for different periods of time followed by quenching to 0 °C which caused reversible shape transformation. Fraction of two-way reversible strain $\varepsilon_{2w}/\varepsilon_t$ is plotted against the annealing time at T_i = 38 °C: it first decreases and then levels off at about 24% of the initial fraction. (b) We also tested the decrease of reversibility during multiple heating−cooling cycles described in Figure 1b−e as a function of cross-linking density as indicated. The sample numbers are consistent with Table 1. As in the annealing-time test, samples were initially programmed to 20% uniaxial extension and then subjected to a series of 10 heating−cooling cycles from T = 0 °C to an intermediate T_i specific to each polymer (**6**, 38 °C; **7**, 41 °C; **9**, 53 °C). The plot shows normalized fraction of two-way reversible strain ($\varepsilon_{2w}/\varepsilon^0_{2w}$) for three polymers as a function of the number of cycles, where ε_{2w} is the strain of two-way reversibility and ε^0_{2w} is the reversible strain of the first cycle. Similar to the annealing time test in part a, reversibility decreases and then levels off. The sample with highest cross-linking density (polymer **9**) shows the smallest decay.

the T_i effect for one material and then the effect of cross-linking for a series of elastomers of the same chemical composition differing in cross-linking density. Figure 2 outlines the interplay of the SM processes for one of the POA elastomers subjected to uniaxial stretching (polymer **10** in Table 1: ν = 620 mol/m^3, T_m = 41 °C). In all three cases (Figure 2a), we start with heating an extended sample (temporary shape) with an initial length of $L = L_t$ from an initial temperature T_0 to an intermediate temperature T_i within the melting interval ($T_0 < T_i < T_f$). Partial melting of crystallites results in contraction of the sample to $L = L_i$ (state 1). From this state, the sample can be further altered in three different ways. First, we can continue heating the sample to a final temperature $T_f \gg T_m$ to complete the melting process and reach nearly 100% recovery of the original shape ($L = L_0$) along with complete relaxation of the chemical network (state 2). This process corresponds to conventional one-way SM, which is irreversible. Second, we can cool the sample to prompt recrystallization of the molten polymer strands confined between the latent crystallites. This step causes two-way reversible elongation to $L = L_{2w}$ (state 3), which can be repeated multiple times as displayed in Figure 1e. In Supporting Information, Figures S3−S5 and Table S1, the results of the AFM and SAXS studies confirm that the crystalline morphology remains largely unchanged over multiple heating and cooling cycles exhibiting full reversibility of crystallite shapes and orientations. Here, the crystallites serve both as seeds and templates[39,40] for recrystallization of the constrained network strands along the promptest pathway replicating the architectural scaffold of the temporary shape. Third, we can manually contract the sample from $L = L_i$ to a new (shorter) length of $L = L_r$ and quench it there (state 4). Subsequent heating first causes elongation of the sample restoring its intermediate shape ($L = L_i$, state 1) followed by its contraction toward the original shape ($L = L_0$, state 2). As mentioned above, the relative contribution of the SM processes depends on the extent of melting; i.e., the temperature T_i reached within the melting interval. This dependence has been thoroughly studied for all synthesized materials (Supporting Information, Figure S6) and outlined in Figure 2b for one particular sample. At any given T_i, total temporary strain $\varepsilon_t = (L_t - L_0)/L_0$ is the sum of strain ε_r released upon heating and strain ε_s stored in the sample ($\varepsilon_t = \varepsilon_r + \varepsilon_s$). Naturally, as a sample recovers upon heating, the fraction of released strain ε_r increases at the expense of stored strain ε_s. Assuming that our materials do not show the uncommon auxetic behavior,[41] the released strain can be represented as the sum $\varepsilon_r = \varepsilon_i + \varepsilon_{2w}$ of irreversible strain ε_i and two-way reversible strain $\varepsilon_{2w} = (L_{2w} - L_i)/L_0$, which can be recovered multiple times upon sequential heating−cooling cycles. With increasing temperature, the contribution of ε_{2w} first increases, reaching maximum at ca. $T_i = T_m$, and then decreases to zero. The stored strain $\varepsilon_s = \varepsilon_{1w} + \varepsilon_n$ has two contributions, where $\varepsilon_{1w} = (L_i - L_{1w})/L_0$ is one-way reversible strain, i.e., strain induced by reverse reprogramming and then recovered during initial heating from T_0 to T_i, and ε_n is strain inaccessible during the reprogramming step. Similar to two-way reversibility, a sample's ability to accomplish one-way reversibility first increases and then decreases with partial melting temperature (T_i). When approaching the stage of complete melting at around T = 50 °C, the sample completely loses memory of its temporary shape and shape recovery becomes irreversible ($\varepsilon \cong \varepsilon_i$).

As such, relative contributions of reversible and irreversible shape transformations are tunable and correlated. For better visualization of the observed correlations, we graphically integrated three conceptually different SM behaviors that can be achieved for any sample at a particular intermediate temperature T_i of partial melting (Figure 2c). Maximum fractions of one-way and two-way reversible strains ($\varepsilon_{1w}/\varepsilon_t$ and $\varepsilon_{2w}/\varepsilon_t$) are achieved at the temperatures $T_i = T_{m1}$ and $T_i = T_{m2}$, respectively. In addition to varying T_i, the ε_{1w} and ε_{2w} fractions can be changed by controlling the heating/cooling rates or duration of isothermal annealing. For example, Figure 3 shows that $\varepsilon_{2w}/\varepsilon_t$ slowly decreases and levels off upon long-time annealing at a constant T_i or, alternatively, is stabilized by increasing the degree of cross-linking. Fast quenching and dense cross-linking enhance two-way reversibility by taking

dx.doi.org/10.1021/ma4023185 | Macromolecules 2014, 47, 1768−1776

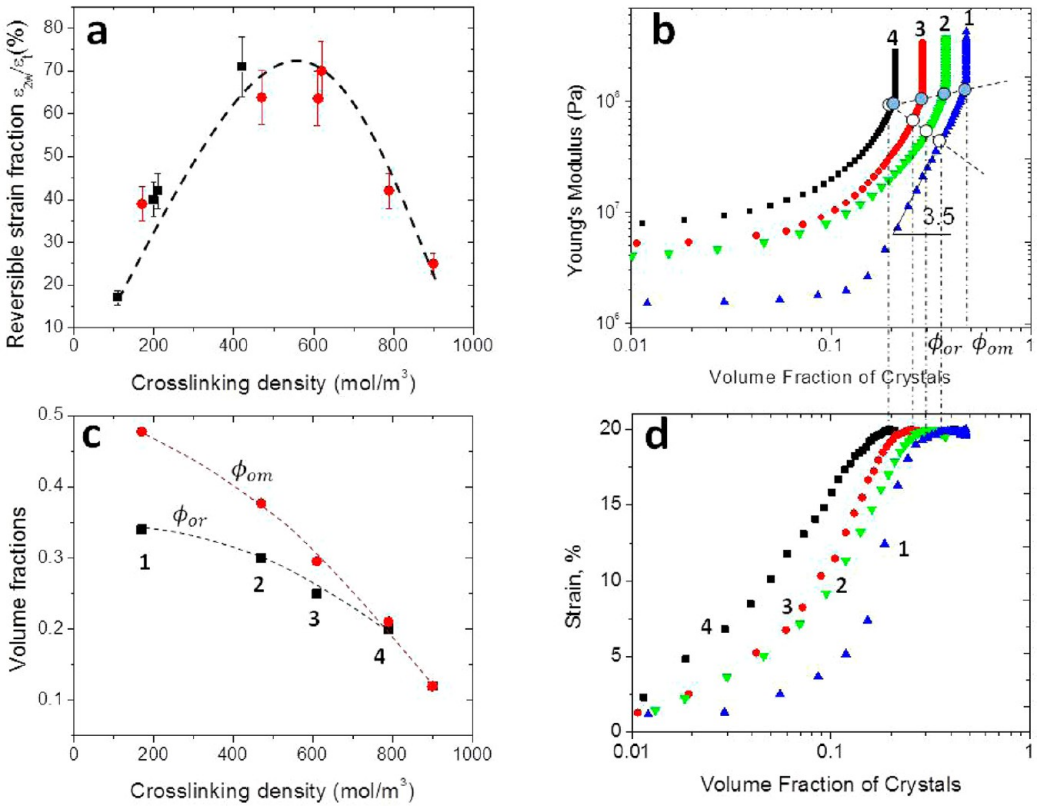

Figure 4. (a) Fraction of two-way reversible strain $\varepsilon_{2w}/\varepsilon_t$ (measured at $T_i = T_{m2}$, see Figure 2c) initially increases with cross-linking density, reaching a maximum value of ca. 70% at $\nu \cong 600$ mol/m^3 and then decreases in highly cross-linked samples. Red and black dots correspond to poly(octlylene adipate) homopolymers and copolymers, respectively (see Figure S1a in Supporting Information). (b) Young's modulus $E(\phi)$ exhibits characteristic decay with decreasing volume fraction ϕ of the crystalline phase upon melting, a quantity which depends on the cross-linking density: (1) $\nu = 170$ mol/m^3, (2) $\nu = 470$ mol/m^3 (3) $\nu = 610$ mol/m^3, and (4) $\nu = 790$ mol/m^3. The solid and open circles indicate the onsets of the melting and shape recovery processes as the volume fraction reaches $\phi = \phi_{om}$ and $\phi = \phi_{or}$, respectively. (c) Volume fractions of the crystalline phase, corresponding to the onset of shape recovery and melting (see panel b), decrease with cross-linking density. (d) Recovery of the original sample length upon melting demonstrates strong correlation with the decrease of the elasticity modulus shown in panel b. The sample numbers in panels c and d are consistent with those in panel b.

advantage of the slow relaxation of the constrained polymer-network strands. This behavior emphasizes the kinetic character of shape-memory reversibility: restoration of the temporary shape is facilitated by chemical cross-links that hinder the relaxation of molten network strands, thus favoring their recrystallization along the fastest pathways to reform the crystalline scaffold of the temporary shape. The kinetic nature of two-way RSM will be further examined through the effect of cross-linking density discussed below.

As seen in Figure 2b, both two-way and one-way reversible strains are always fractions of the total strain, i.e., $\varepsilon_{2w} < \varepsilon_t$ and $\varepsilon_{1w} < \varepsilon_t$. This poses an important question: How can one control and ultimately maximize the range of reversible strain? The answer to this question lies in the competition between the chemical network and crystalline scaffold. To understand this competition in a quantitative fashion, we have studied the effect of cross-linking on two-way reversibility by analyzing the effect of cross-linking density on the $\varepsilon_{2w}/\varepsilon_t$ ratio. In general, chemical cross-links have a dual effect on shape-memory properties: First, the elastic modulus of an elastomer increases with cross-linking density, and a higher modulus favors recovery of the original shape upon melting. Second, chemical cross-links frustrate the crystallization process and lower the degree of crystallinity, hence, impeding the ability of crystallites to encode the temporary shape. The result of these competing effects is demonstrated in Figure 4a, which shows the fraction of reversible strain $\varepsilon_{2w}/\varepsilon_t$ increasing to almost 70% as the cross-linking density reaches ca. 600 mol/m^3 followed by a decline in $\varepsilon_{2w}/\varepsilon_t$ for strongly cross-linked samples. The initial increase in reversibility is due to enhancement of the templating effect of the latent crystallites: molten polymer strands in strongly cross-linked elastomers exhibit slow relaxation and upon heating, they largely remain in place, and thus they are available to template recrystallization (on typical experimental time scales t < 1 h). The decrease in reversibility in strongly cross-linked materials is simply due to the inability of sparse crystallites to secure a temporary shape due to the lack of percolation of the crystalline domains across the sample.

To further demonstrate the dual effect of cross-linking density on shape memory, we have plotted the Young's modulus (tensile storage modulus E measured at $f = 1$ Hz) as a function of volume fraction of the crystalline phase measured during a shape recovery process upon melting (Figure 4b). This plot was obtained by correlating data from DSC and DMA tests on the same samples (Supporting Information, Figure S7). Figure 4b combines four $E(\phi)$ data sets corresponding to four chemically identical elastomers with different cross-linking densities. The data sets exhibit consistent offsets along both axes, i.e., modulus (y-axis) and volume fraction (x-axis). The low-ϕ offsets along the x-axis correspond to the decrease of

dx.doi.org/10.1021/ma4023185 | Macromolecules 2014, 47, 1768−1776

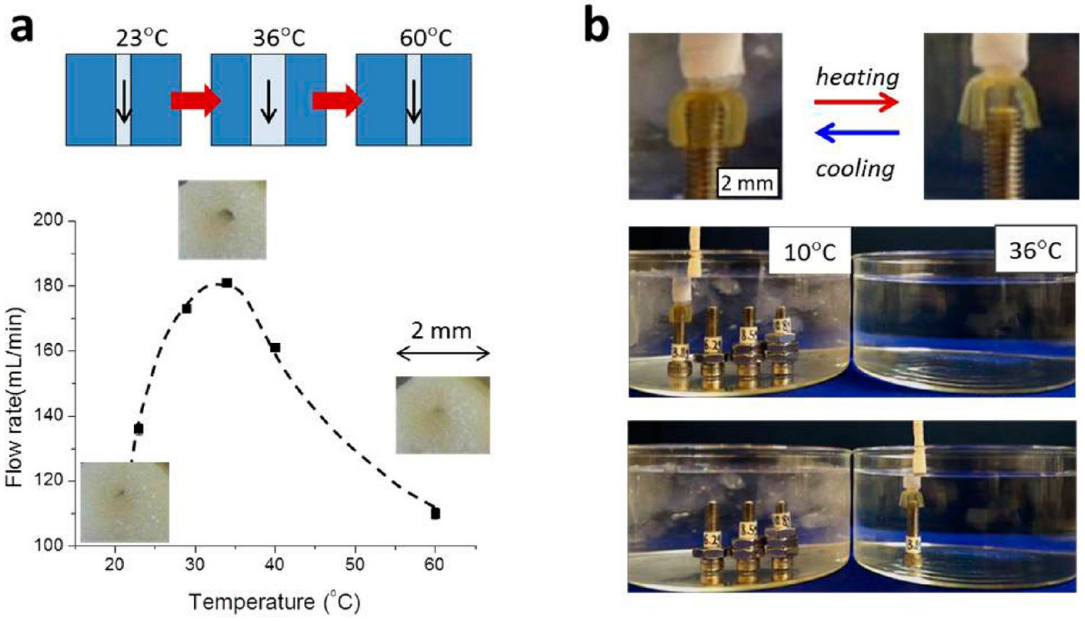

Figure 5. (a) Water flow changes upon heating through an aperture within a shape-memory elastomer (polymer **6** in Table 1, ν = 200 mol/m^3, T_m = 42 °C), which was programmed to perform one-way reversibility. Upon heating the sample from 23 to 60 °C, the aperture first opens at T = 36 °C and then again closes at T = 60 °C. From the Hagen−Poiseuille equation for the flow rate, we determined an aperture radius of R = 0.34 mm, which was consistent with optical micrographs. (b) A soft gripper was designed from a shape-memory polymer, which was programmed to perform two-way reversibility. The gripper closes and opens during cooling−heating cycles, respectively. The gripper was used to move different weights (bolt and nut assemblies) from cold (10 °C) to warm (36 °C) water reservoirs (video in the Supporting Information).

degree of crystallinity with cross-linking density, while the high-E shifts along the y-axis are due to the increase of the elastic modulus with increasing cross-linking density. This plot also depicts two characteristic volume fractions $\phi = \phi_{om}$ (solid circle) and $\phi = \phi_{or}$ (open circle) that correspond to onsets of the melting and shape recovery processes, respectively. Note that depending on the degree of cross-linking, shape recovery may fall substantially behind the onset of melting. For example, in Figure 4b, the elastomer with the lowest cross-linking density exhibits shape variations after melting of ca. 30% v/v of the crystalline phase. The difference $\phi_{om} - \phi_{or} \cong 0.3$ corresponds to fraction of "redundant" crystals that are not necessary for securing a temporary shape. It is also interesting to see that the onsets of these two different processes converge with increasing degree of cross-linking, which favorably correlates with the enhancement of reversibility in Figure 4a. We have plotted the two volume fractions (ϕ_{om} and ϕ_{or}) as a function of the cross-linking density (Figure 4c) to display this observation: effectiveness of shape reversibility (Figure 4a) correlates with the material's ability to secure and restore shapes (Figure 4c). Therefore, it is vital to optimize the cross-linking density. On the one hand, cross-linking should provide sufficient network strength for shape recovery and sufficient constraints for self-templating crystallization; On the other hand, cross-linking should not be too high to allow for sufficient crystallinity to secure a temporary shape and develop a percolated scaffold. The maximum reversibility is achieved with a cross-linking density n^*, an upper limit which allows for a minimum degree of crystallinity necessary to secure the temporary shape while providing sufficient constraints for polymer strands in the partially molten state to facilitate their recrystallization toward the original shape.

Another curious behavior shown by the plot in Figure 4b is a characteristic scaling relation $E \sim \phi^b$ between the modulus and volume fraction of the crystalline phase. This correlation is especially distinct for samples with lower cross-linking densities, which exhibit less constrained crystallization (see Supporting Information, Figure S8 for additional samples). The unique scaling relation can be explained with a composite model for semicrystalline elastomers consisting of fillers (clusters of crystallites, e.g. spherulites) embedded in the continuous matrix of a chemical network.[42,43] As discussed in Supporting Information (Figures S9 and S10), depending on the cluster morphology, there is another scaling relation $\phi_{cluster} \sim \phi^a$ between the volume fraction of clusters and crystallites, which gives $E \sim \phi_{cluster}^{b/a}$. Studies of these interesting correlations are outside the scope of the present paper and will be studied separately. However, we can correlate the modulus decrease observed in Figure 4b with recovery of the original sample length shown by Figure 4d. The significant (ca. 40×) decrease in modulus exhibited by sample **1** in the scaling regime is accompanied by significant (ca. 60%) alteration of the sample shape. We conjecture that mesoscopic clusters of crystallites provide an effective translation from the microscopic structure of the elastomer to the macroscopic shape, and allow more efficient fastening and restoration of shapes.

As mentioned in the Introduction, reversible shape memory is very appealing for many practical applications.[15,44] Both one-way and two-way reversible shape memory points to practical applications that are particular for each type. The unique feature of one-way reversibility is that it occurs upon heating only and all three shapes (one permanent and two temporary ones) are stable at any given temperature below the interval of melting. Even though one-time reversibility can occur only once, the heating-only protocol opens an interesting niche for practical applications that require reversible shape changes on demand and in discrete steps. For example, the reversible coil-line shape transformations in Figure 1f,g suggest that one-way

dx.doi.org/10.1021/ma4023185 | Macromolecules 2014, 47, 1768−1776

reversibility can be used for minimally invasive insertion and removal of medical implants, such as stents. Because of the heating-only protocol, it is possible to insert and expand a stent at a temperature of, e.g., T_1 = 36 °C and then to shrink and remove the stent significantly later (after many months) by heating to a higher temperature of, e.g., T_2 = 42 °C. In addition to shape-active implants, we can use one-way reversibility to reversibly control flow through an aperture or a catheter.[29] Figure 5a demonstrates a proof of concept of this application. A thick film of a shape memory elastomer was perforated to have a hole of R = 0.5 mm and then programmed to perform one-way reversible changes of the aperture. This film was inserted into a microfluidic device which maintains a constant pressure gradient and allows temperature variations. As shown in Figure 5a, upon heating the system the aperture first opens resulting in the corresponding increase of the flow rate, and then contracts slowing down the flow. From the Hagen−Poiseuille equation for the flow rate under a controlled pressure gradient $\nabla P = 10^4$ N/m^3, we have determined an aperture radius of R = 0.34 mm, which is consistent with optical micrographs.

Applications of two-way reversible SMPs are quite straightforward and in line with other stimuli responsive systems like hydrogels and electrically active polymers.[1,2,11] However, the advantage of shape memory polymers over other shape-responsive systems is the ability to adopt and routinely control complex shapes. An additional advantage of the two-way reversible systems discussed here is their ability to perform a nearly infinite number of shape-transformation cycles completely autonomously, i.e. without application of an external force. The origami in Figure 1d was used as a gripper to move objects between cold (10 °C) and warm (36 °C) water reservoirs (Figure 5b), and a complete process can be viewed in the video in the Supporting Information. The objects varied in mass up to 10 g, while the gripper was weighed 0.1 g. As such, the maximum achieved payload-to-weight ratio is 100, which is higher than many industrial robotic grippers.[45] For example, the payload-to-weight ratio of ROBOTIQ robotic grippers is lower than 5.

CONCLUSION

In summary, we have explored a general mechanism of reversible shape memory in semicrystalline elastomers, which integrates three conceptually different shape memory protocols: (i) one-way irreversible, (ii) one-way reversible, and (iii) two-way reversible shape transformations. Semicrystalline elastomers with a synthetically tunable combination of chemical cross-links and physical network of crystallites may be viewed as dual-network materials, wherein each network is designed to secure a different shape. Chemical cross-links hold the memory of the original shape, while the physical network of crystallites constructs a scaffold of the temporary shape. While thermodynamics drives relaxation of the chemical network toward the original shape, crystallization of confined and constrained polymer chains is biased toward fastest pathways during cooling guided by the remaining crystallites to the opposite direction to restore the temporary shape. Maximum performance of each individual protocol can be achieved by tuning the cross-linking density and the degree of crystallinity of semicrystalline elastomers. We have shown that the two-way reversible shape memory behavior is a consequence of interplay between the thermodynamics of the chemical network and kinetics of crystallization within a semicrystalline elastomer. While two-way reversibility requires substantial melting to realize a measurable shape shift, the programming of one-way reversibility needs incremental melting to maintain the temporary shape. Further optimization of the reversible shape memory may be achieved by tuning chemical composition and widening the melting temperature interval, but the variety of the RSM behaviors studied in this paper obeys the same universal mechanism as discussed above.

ASSOCIATED CONTENT

Supporting Information

Detailed properties of characterized materials, AFM and SAXS analysis on two-way reversiblilty, analysis on variation of degree of crystallinity, kinetic effect on reversibility and composite model of crystalline network, and a video showing a practical use of the polymer. This material is available free of charge via the Internet at http://pubs.acs.org.

AUTHOR INFORMATION

Corresponding Author

*(S.S.S.) E-mail: sergei@email.unc.edu.

Author Contributions

⊥J.Z. and Q.L. performed the experiments, S.A.T., S.M.B., and Q.L. synthesized materials, J.-M.Y.C. and A.V.D performed theoretical analysis, O.G. and D.N. performed SAXS measurements, V.S.A. discussed results and contributed to the revisions, and S.S.S. composed the manuscript and supervised the project.

Notes

The authors declare no competing financial interests.

ACKNOWLEDGMENTS

The authors thank E. T. Samulski for insightful discussions and reviewing the paper. S.S., A.V.D., and V.S.A. acknowledge financial support from the National Science Foundation DMR-1122483, DMR-1004576, and DMR-1206957. Research carried out at the Center for Functional Nanomaterials (CFN) and National Synchrotron Light Source (NSLS) at the Brookhaven National Laboratory has been supported by the U.S. Department of Energy, Office of Basic Energy Sciences, under Contract DE-AC02-98CH10886.

REFERENCES

(1) Yoshida, R.; Uchida, K.; Kaneko, Y.; Sakai, K.; Kikuchi, A.; Sakurai, Y.; Okano, T. *Nature* **1995**, *374* (6519), 240−242.
(2) Osada, Y.; Matsuda, A. *Nature* **1995**, *376* (6537), 219−219.
(3) Hao, J. K.; Weiss, R. A. *ACS Macro Lett.* **2013**, *2* (1), 86−89.
(4) Skrzeszewska, P. J.; Jong, L. N.; de Wolf, F. A.; Stuart, M. A. C.; van der Gucht, J. *Biomacromolecules* **2011**, *12* (6), 2285−2292.
(5) Therien-Aubin, H.; Wu, Z. L.; Nie, Z. H.; Kumacheva, E. *J. Am. Chem. Soc.* **2013**, *135* (12), 4834−4839.
(6) White, E. M.; Yatvin, J.; Grubbs, J. B.; Bilbrey, J. A.; Locklin, J. *J. Polym. Sci., Part B: Polym. Phys.* **2013**, *51* (14), 1084−1099.
(7) Camacho-Lopez, M.; Finkelmann, H.; Palffy-Muhoray, P.; Shelley, M. *Nat. Mater.* **2004**, *3* (5), 307−310.
(8) Yu, H. F.; Ikeda, T. *Adv. Mater.* **2011**, *23* (19), 2149−2180.
(9) Yang, Z. Q.; Huck, W. T. S.; Clarke, S. M.; Tajbakhsh, A. R.; Terentjev, E. M. *Nat. Mater.* **2005**, *4* (6), 486−490.
(10) Ohm, C.; Serra, C.; Zentel, R. *Adv. Mater.* **2009**, *21* (47), 4859−4862.
(11) Koerner, H.; Price, G.; Pearce, N. A.; Alexander, M.; Vaia, R. A. *Nat. Mater.* **2004**, *3* (2), 115−120.
(12) Hsiao, B. S.; Gardner, K. H.; Wu, D. Q.; Chu, B. *Polymer* **1993**, *34* (19), 3986−3995.
(13) Lendlein, A.; Jiang, H. Y.; Junger, O.; Langer, R. *Nature* **2005**, *434* (7035), 879−882.

(14) Yu, Y. L.; Nakano, M.; Ikeda, T. *Nature* **2003**, *425* (6954), 145−145.
(15) Behl, M.; Razzaq, M. Y.; Lendlein, A. *Adv. Mater.* **2010**, *22* (31), 3388−3410.
(16) Xie, T. *Nature* **2010**, *464* (7286), 267−270.
(17) Mather, P. T.; Luo, X. F.; Rousseau, I. A. *Annu. Rev. Mater. Res.* **2009**, *39*, 445−471.
(18) Liu, C.; Qin, H.; Mather, P. T. *J. Mater. Chem.* **2007**, *17* (16), 1543−1558.
(19) Sun, L.; Huang, W. M.; Ding, Z.; Zhao, Y.; Wang, C. C.; Purnawali, H.; Tang, C. *Mater. Des.* **2012**, *33*, 577−640.
(20) Li, G.; Fei, G. X.; Xia, H. S.; Han, J. J.; Zhao, Y. *J. Mater. Chem.* **2012**, *22* (16), 7692−7696.
(21) Meng, H.; Li, G. Q. *Polymer* **2013**, *54* (9), 2199−2221.
(22) Yakacki, C. M.; Gall, K. Shape-Memory Polymers for Biomedical Applications. In *Shape-Memory Polymers*; Advances in Science 226; Springer: Berlin, **2010**; pp 147−175.
(23) Zhu, Z. C.; Senses, E.; Akcora, P.; Sukhishvili, S. A. *ACS Nano* **2012**, *6* (4), 3152−3162.
(24) Benkoski, J. J.; Breidenich, J. L.; Uy, O. M.; Hayes, A. T.; Deacon, R. M.; Land, H. B.; Spicer, J. M.; Keng, P. Y.; Pyun, J. *J. Mater. Chem.* **2011**, *21* (20), 7314−7325.
(25) Chen, Y. L.; Kushner, A. M.; Williams, G. A.; Guan, Z. B. *Nature Chem.* **2012**, *4* (6), 467−472.
(26) Chung, T.; Rorno-Uribe, A.; Mather, P. T. *Macromolecules* **2008**, *41* (1), 184−192.
(27) Pandini, S.; Passera, S.; Messori, M.; Paderni, K.; Toselli, M.; Gianoncelli, A.; Bontempi, E.; Ricco, T. *Polymer* **2012**, *53* (9), 1915−1924.
(28) Behl, M.; Kratz, K.; Zotzmann, J.; Nochel, U.; Lendlein, A. *Adv. Mater. (Deerfield Beach, Fla.)* **2013**, *25* (32), 4466−9.
(29) Qin, H. H.; Mather, P. T. *Macromolecules* **2009**, *42* (1), 273−280.
(30) Ge, Q.; Westbrook, K. K.; Mather, P. T.; Dunn, M. L.; Qi, H. J. *Smart Mater. Struct.* **2013**, *22* (5), 055009.
(31) Westbrook, K. K.; Mather, P. T.; Parakh, V.; Dunn, M. L.; Ge, Q.; Lee, B. M.; Qi, H. J. *Smart Materi. Struct.* **2011**, *20* (6), 065010-1−065010-9.
(32) Behl, M.; Kratz, K.; Noechel, U.; Sauter, T.; Lendlein, A. *Proc. Natl. Acad. Sci. U.S.A.* **2013**, *110* (31), 12555−12559.
(33) Serrano, M. C.; Ameer, G. A. *Macromol. Biosci.* **2012**, *12* (9), 1156−1171.
(34) Brosnan, S. M.; Brown, A. H.; Ashby, V. S. *J. Am. Chem. Soc.* **2013**, *135* (8), 3067−3072.
(35) Heuchel, M.; Sauter, T.; Kratz, K.; Lendlein, A. *J. Polym. Sci., Part B: Polym. Phys.* **2013**, *51* (8), 621−637.
(36) Lendlein, A.; Sauter, T. *Macromol. Chem. Phys.* **2013**, *214* (11), 1175−1177.
(37) Kratz, K.; Madbouly, S. A.; Wagermaier, W.; Lendlein, A. *Adv. Mater.* **2011**, *23* (35), 4058−4062.
(38) Behl, M.; Lendlein, A. *J. Mater. Chem.* **2010**, *20* (17), 3335−3345.
(39) Fillon, B.; Wittmann, J. C.; Lotz, B.; Thierry, A. *J. Polym. Sci., Part B: Polym. Phys.* **1993**, *31* (10), 1383−1393.
(40) Xu, J. J.; Ma, Y.; Hu, W. B.; Rehahn, M.; Reiter, G. *Nat. Mater.* **2009**, *8* (4), 348−353.
(41) Franke, M.; Magerle, R. *ACS Nano* **2011**, *5* (6), 4886−4891.
(42) Christensen, R. M. *J. Mech. Phys. Solids* **1990**, *38* (3), 379−404.
(43) Raos, G. *Macromol. Theory Simul.* **2003**, *12* (1), 17−23.
(44) Lendlein, A.; Langer, R. *Science* **2002**, *296* (5573), 1673−1676.
(45) Kolluru, R.; Valavanis, K. P.; Smith, S. A.; Tsourveloudis, N. *IEEE Trans. Syst. Man Cybernetics Part a: Syst. Hum.* **2000**, *30* (2), 181−187.